Supporting Information

High-Performance Liquid Metal/Polyborosiloxane Elastomer towards Thermally Conductive Applications

Chunyu Zhao, Yu Wang, Liang Gao, Yunqi Xu, Ziyang Fan, Xujing Liu, Yong Ni, Shouhu Xuan, Huaxia Deng* and Xinglong Gong**

CAS Key Laboratory of Mechanical Behavior and Design of Materials, Department of Modern Mechanics, University of Science and Technology of China (USTC), Hefei 230027, P. R. China.

**Corresponding author:*

wyu@ustc.edu.cn (Y. Wang), hxdeng@ustc.edu.cn (H.X. Deng), gongxl@ustc.edu.cn (X.L. Gong)

Volume fraction of LM [%]	Mass fraction of LM [%]
0.00	0.00
1.00	5.80
5.00	24.30
10.00	40.40
15.00	51.84

Table S1. The correspondence between the volume fraction and mass fraction of LM.

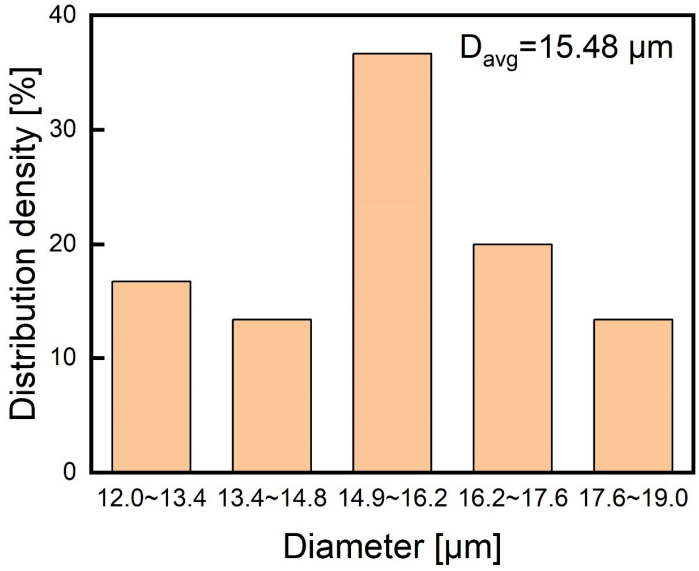

Figure S1. The diameter distribution of LM droplets. The average diameter of the LM droplets was 15.48 μm.

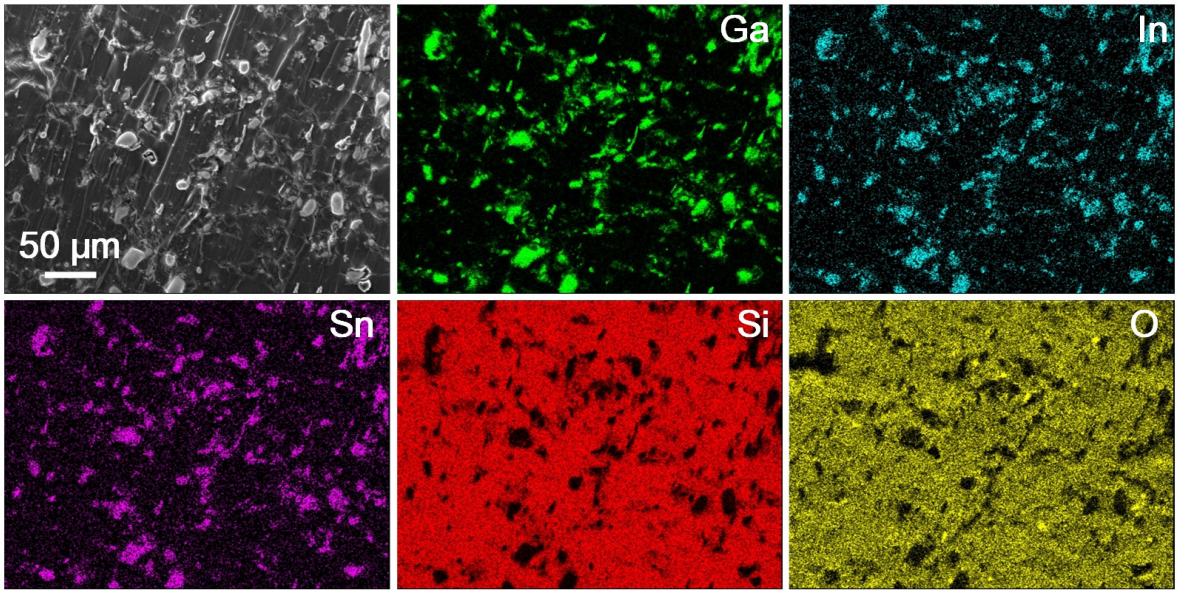

Figure S2. The energy dispersive spectrometer (EDS) mapping of LM/PBSE, and the related element mapping of Ga, In, Sn, Si, and O.

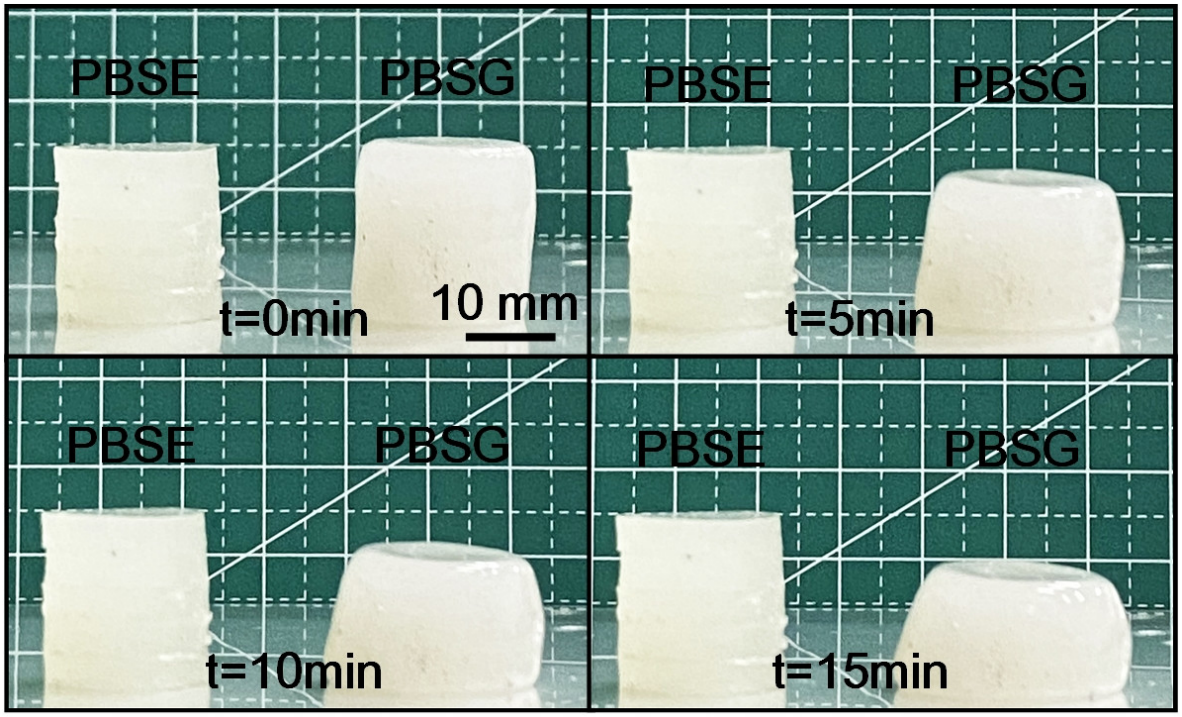

Figure S3. The comparison of the cold flow effect for PBSE and PBSG.

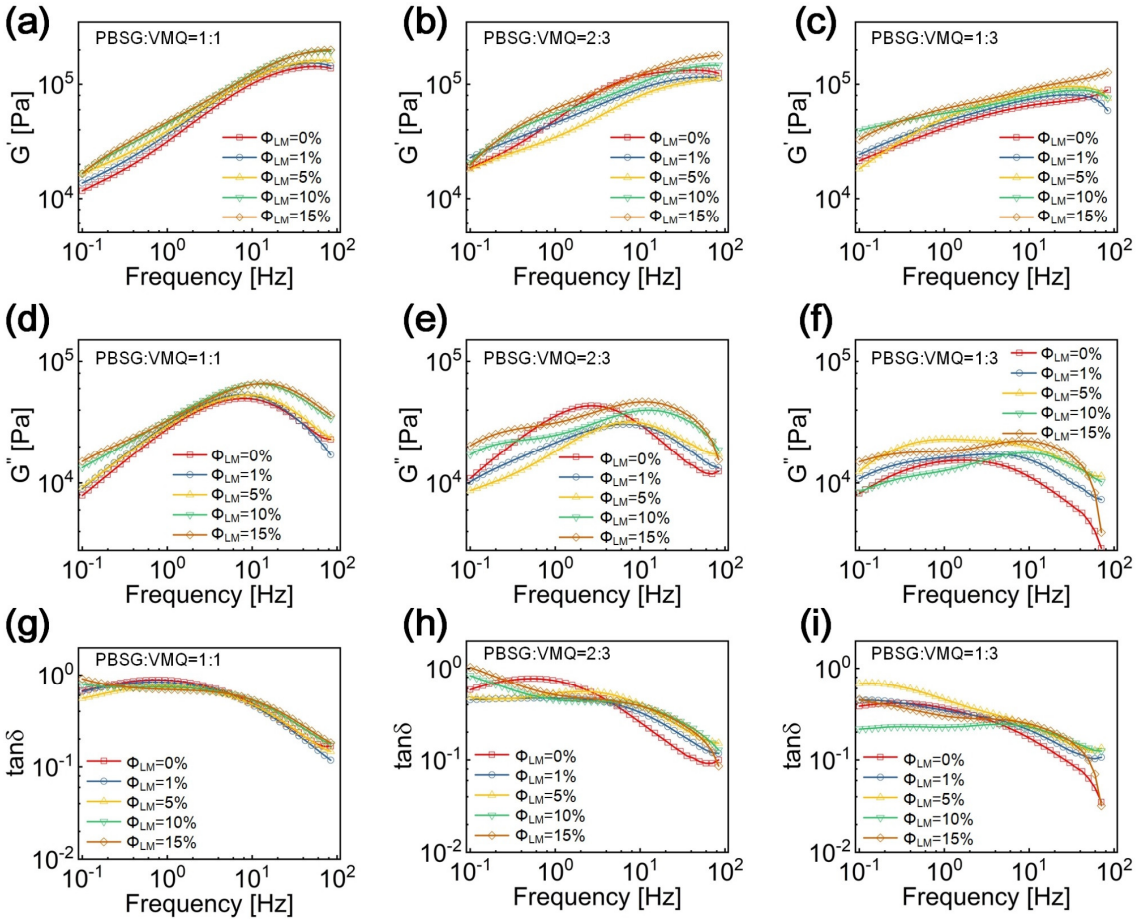

Figure S4. The rheological testing of LM/PBSE specimens with different matrixes and LM volume fractions. (**a-c**) Storage modulus (G') versus frequency curves; (**d-f**) Loss modulus (G'') versus frequency curves; (**g-i**) Loss factor ($\tan\delta$) versus frequency curves.

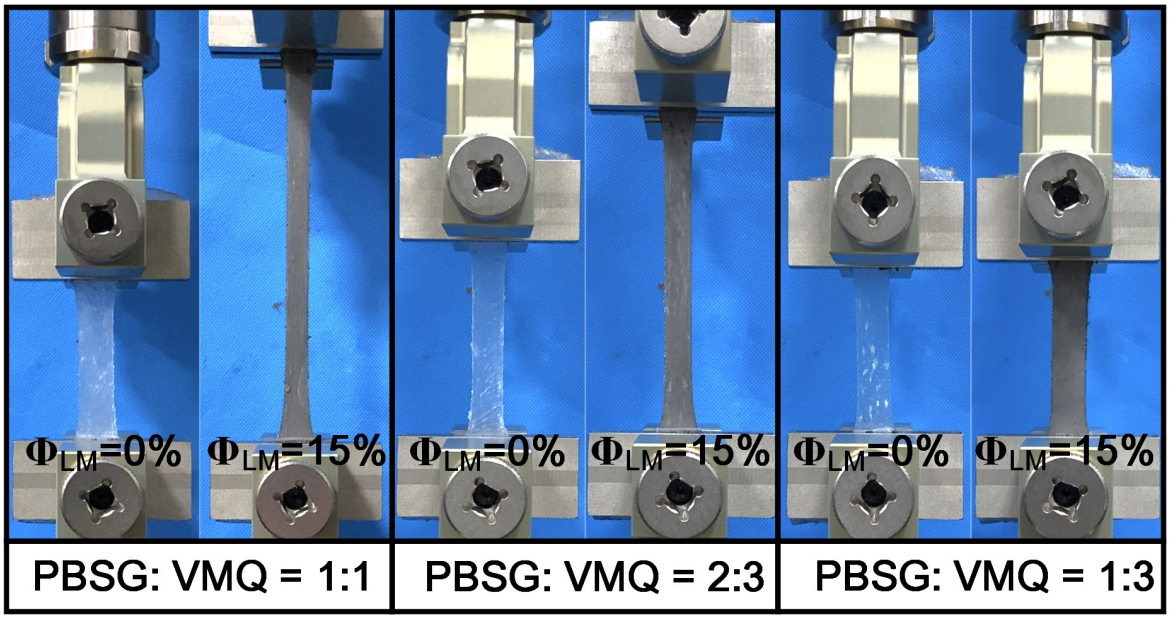

Figure S5. The images of specimens of Φ_{LM} = 0% and Φ_{LM} = 15% LM/PBSE specimens with different matrixes before fracture strain.

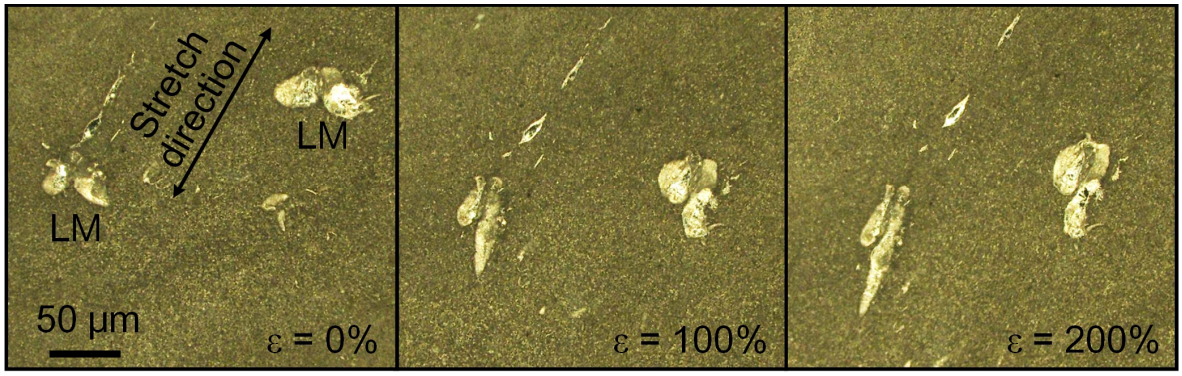

Figure S6. The microscopic structure of the LM droplets during the uniaxial tension process.

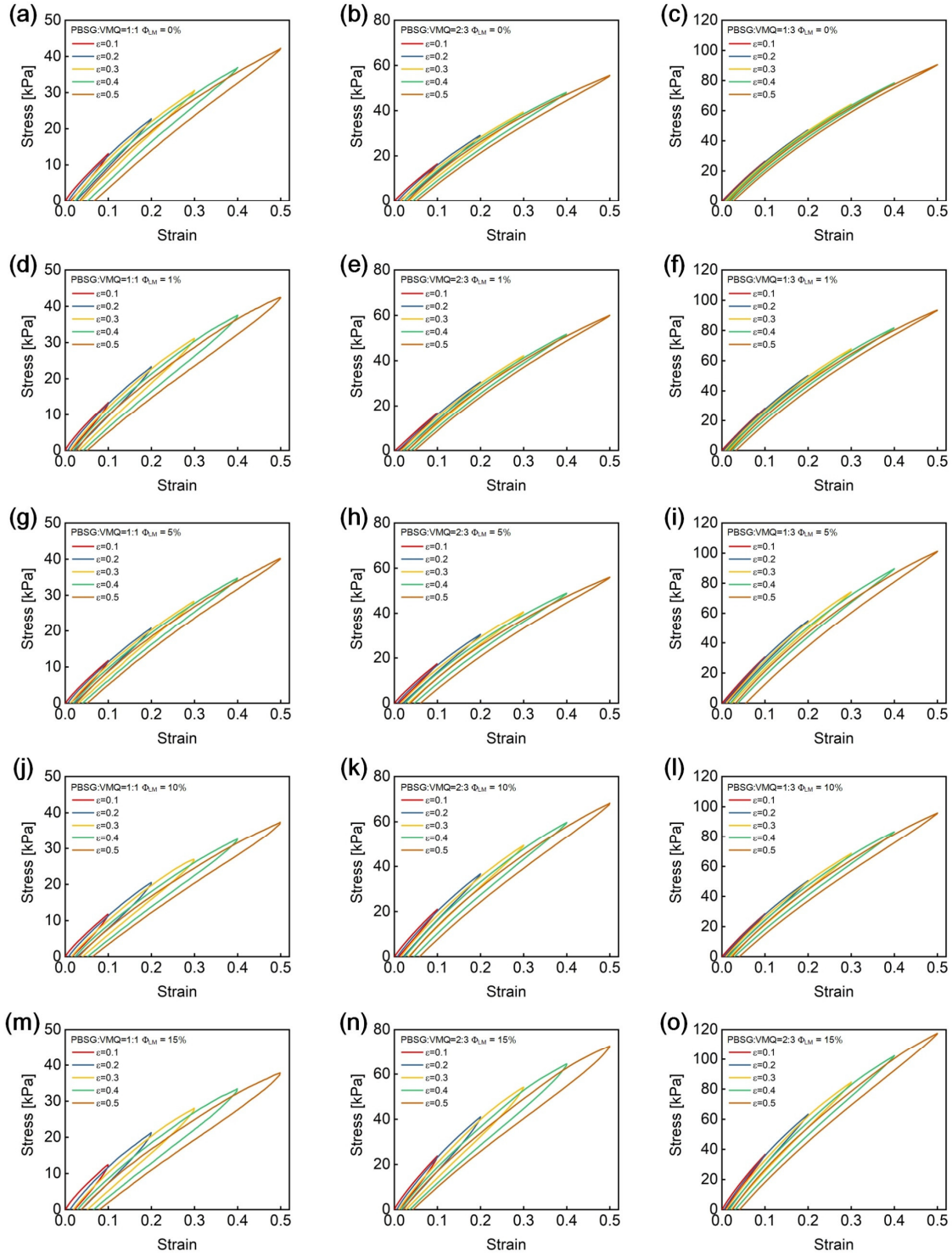

Figure S7. The uniaxial cycling loading test for the LM/PBSE specimens with different matrixes under different strain amplitudes. (**a-c**) Φ_{LM} = 0%; (**d-f**) Φ_{LM} = 1%; (**g-i**) Φ_{LM} = 5%; (**j-l**) Φ_{LM} = 10%; (**m-o**) Φ_{LM} = 15%.

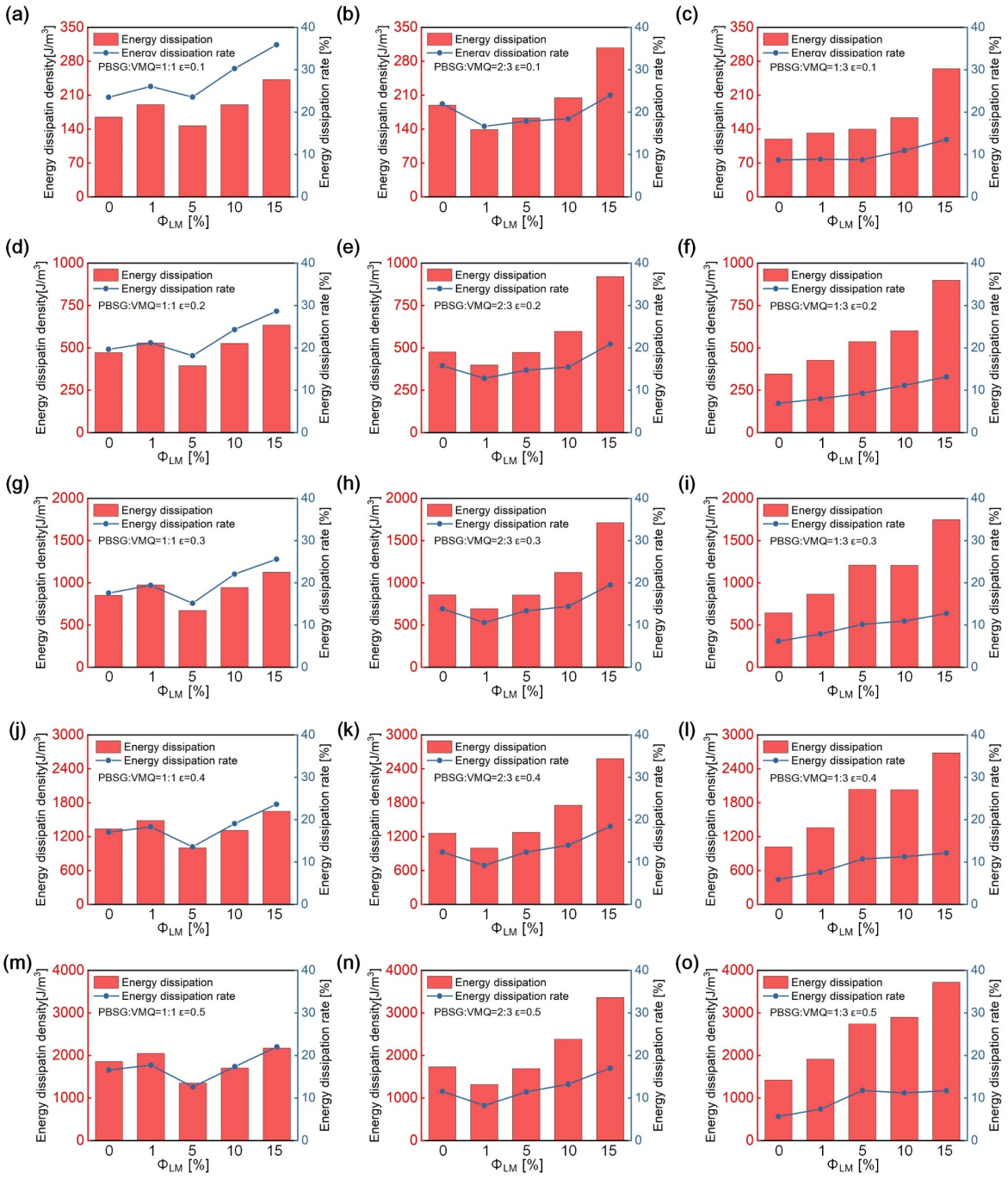

Figure S8. The energy dissipation density and energy dissipation rate for the LM/PBSE specimens with different Φ_{LM} for different matrixes. (**a-c**) ε= 0.1; (**d-f**) ε= 0.2; (**g-i**) ε= 0.3; (**j-l**) ε= 0.4; (**m-o**) ε= 0.5 (The energy dissipation density was defined as the area of the stress hysteresis loop in the stress-strain curve, and the energy dissipation rate was defined as the ratio of the energy dissipation density to the area of the stress-strain curve in the loading stage).

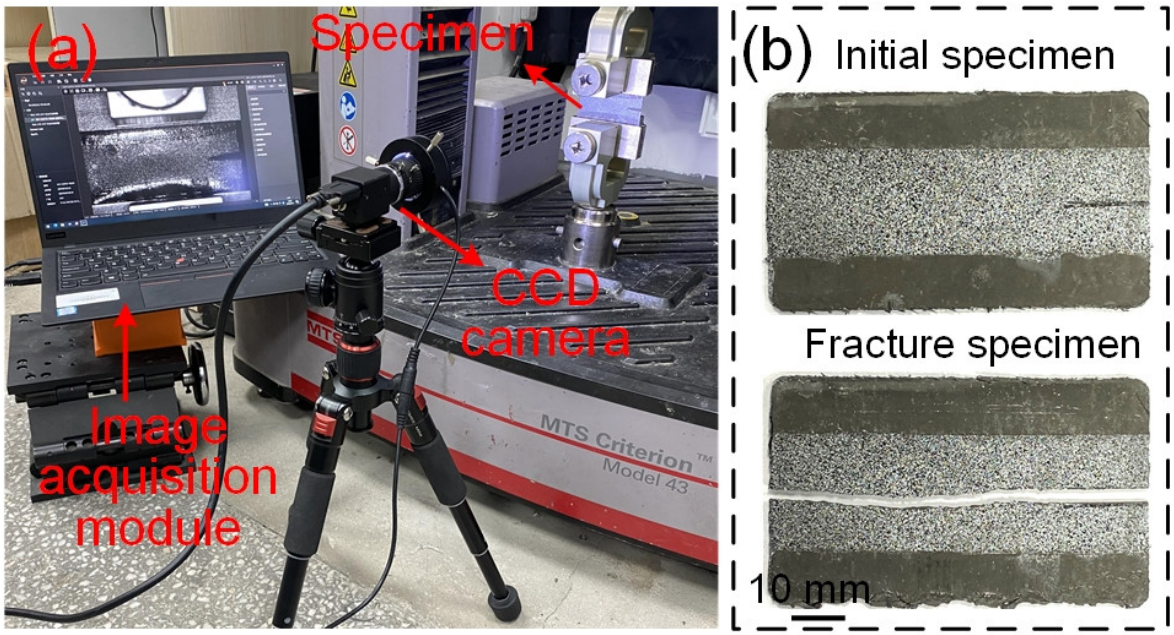

Figure S9. (a) The diagram of the experimental device for crack propagation test; **(b)** The representative morphology of specimens in the initial state and fracture state.

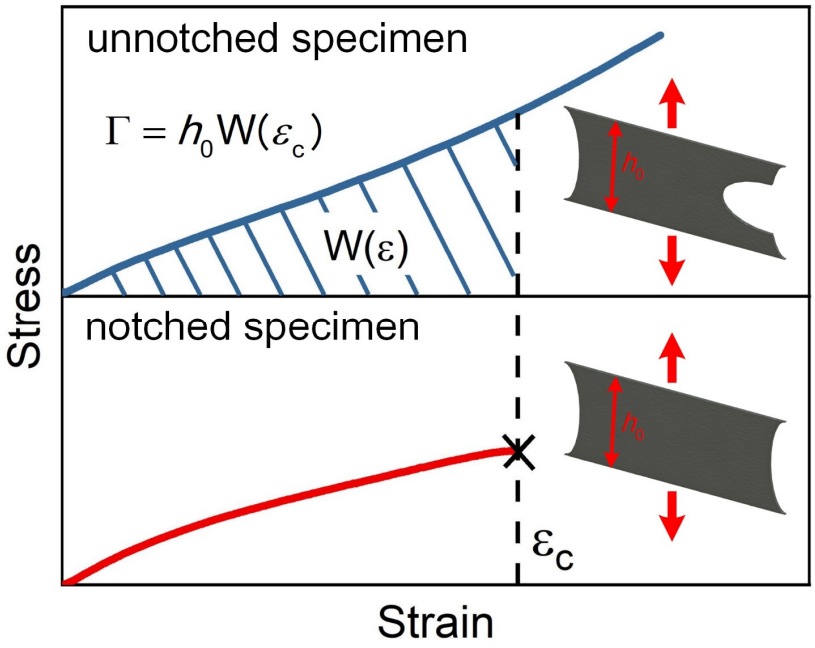

Figure S10. The definition of the fracture toughness (Γ) of the LM/PBSE specimen.

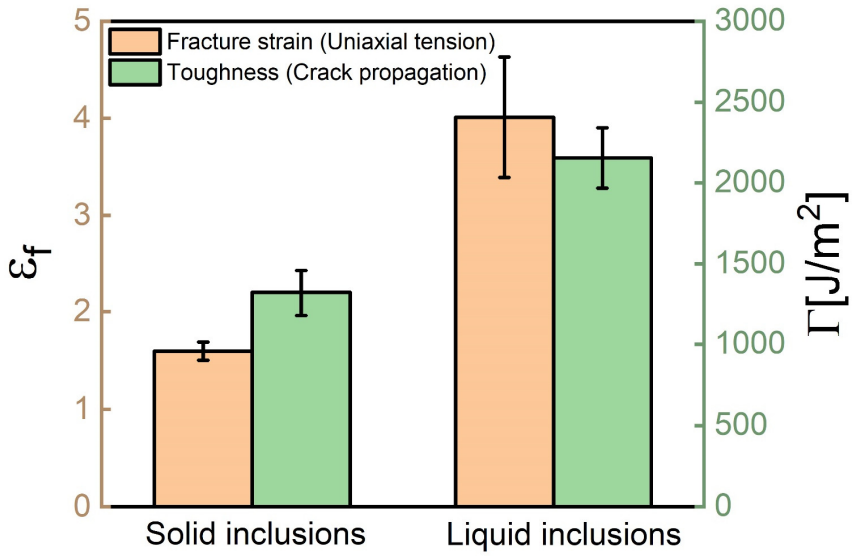

Figure S11. The comparison of fracture strain (ε_f) and toughness (Γ) of solid inclusions (LM with a melting point of 60°C) and room-temperature liquid inclusions LM.

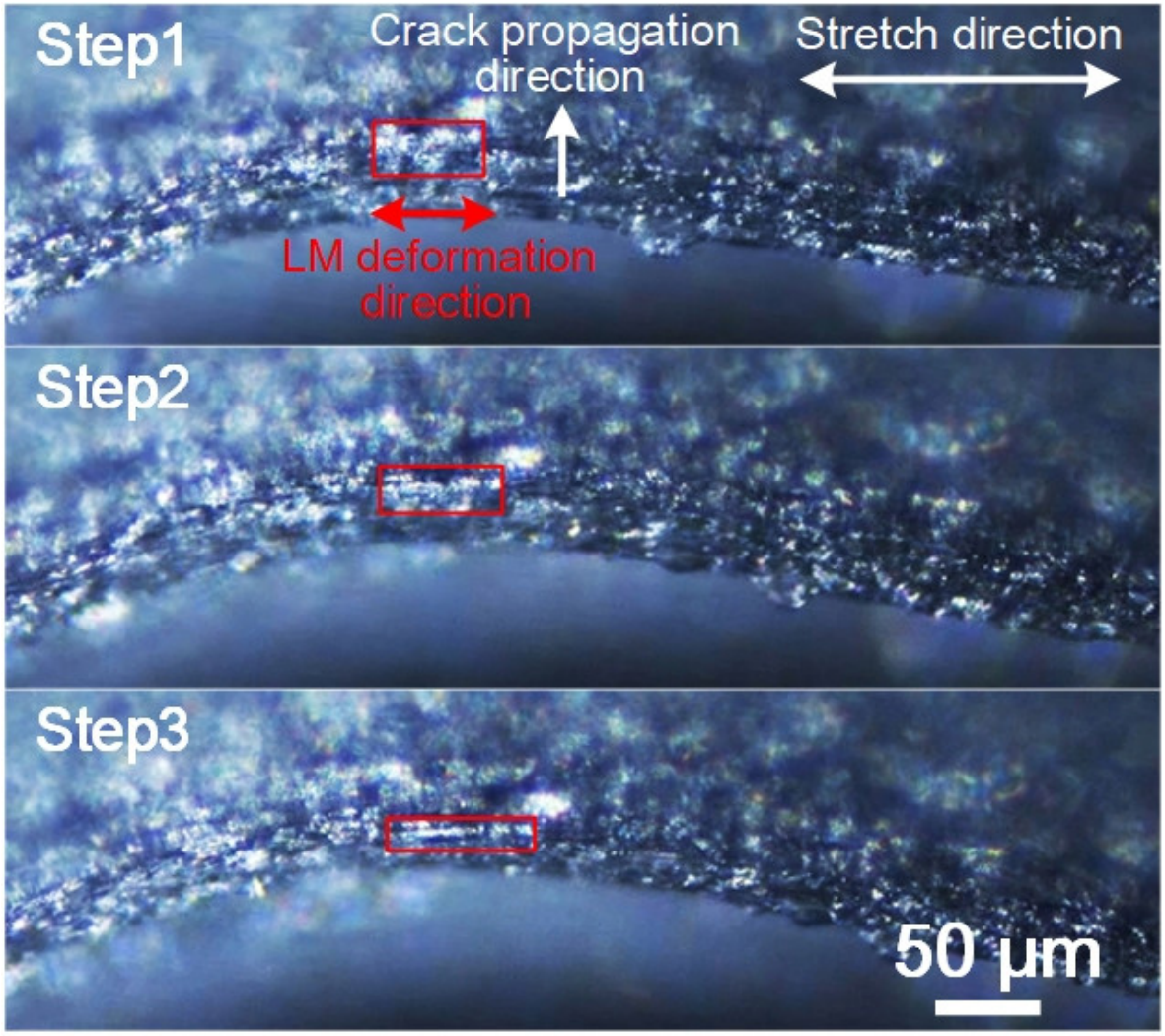

Figure S12. The *in-situ* observation during the crack propagation process. The red region represented the elongation of the LM droplets at the crack tip.

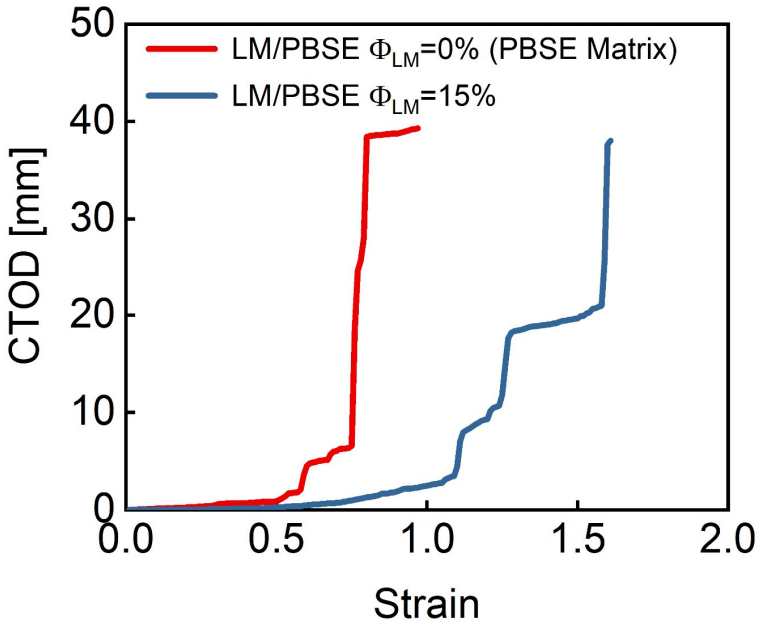

Figure S13. The comparison of the CTOD for pure PBSE matrix (PBSG: VMQ = 1:1, Φ_{LM} = 0%) and LM/PBSE elastomer (PBSG: VMQ = 1:1, Φ_{LM} = 15%).

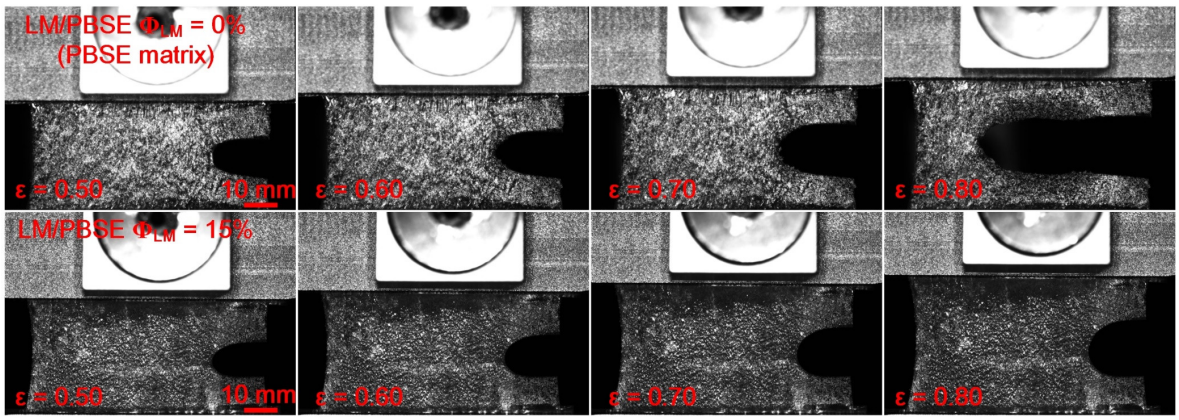

Figure S14. The comparison of the crack morphology for pure PBSE matrix (PBSG: VMQ = 1:1, Φ_{LM} = 0%) and LM/PBSE elastomer (PBSG: VMQ = 1:1, Φ_{LM} = 15%) from ε=0.50 to ε=0.80.

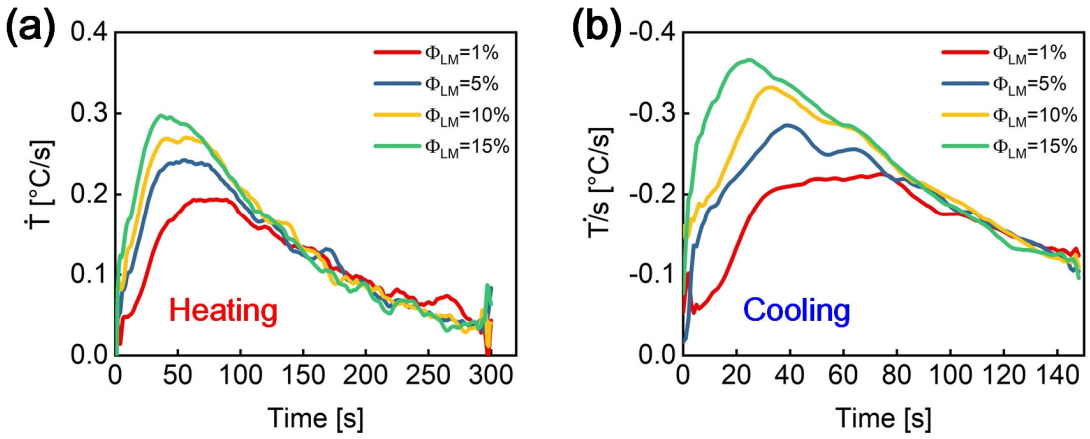

Figure S15. The rate of temperature change of specimens for the matrix PSBG: VMQ=1:1 with different LM volume fractions (Φ_{LM}=1%, 5%, 10%, 15%). **(a)** Heating process; **(b)** Cooling process.

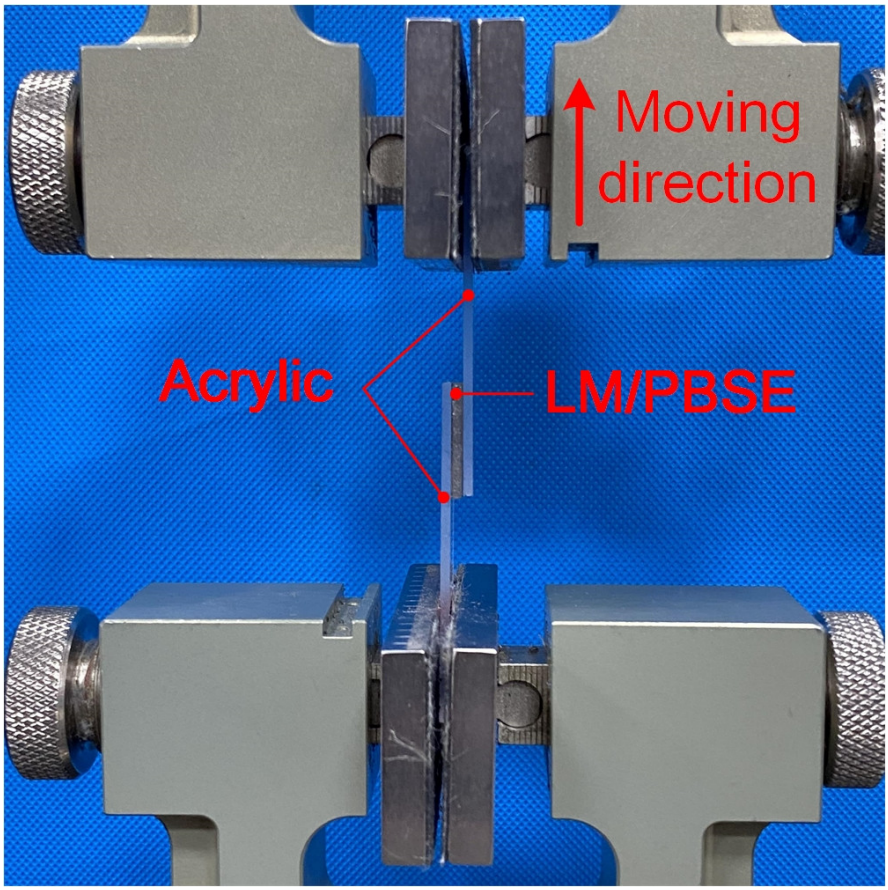

Figure S16. The diagram of the lap-shear experiment.

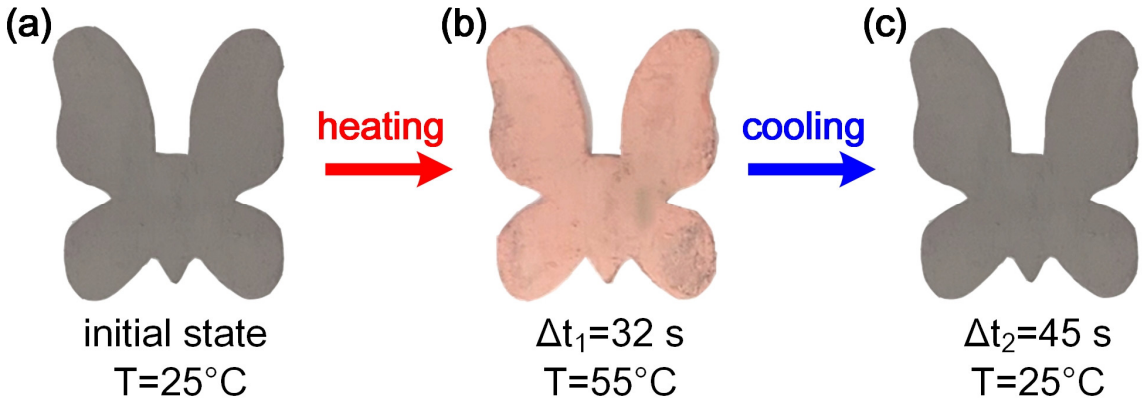

Figure S17. The reversible ability of the color conversion of the LM/PBSE butterfly. **(a)** The initial state of the butterfly; **(b)** The heating process of the butterfly above T_{tran}; **(c)** The cooling process of the butterfly below T_{tran}.

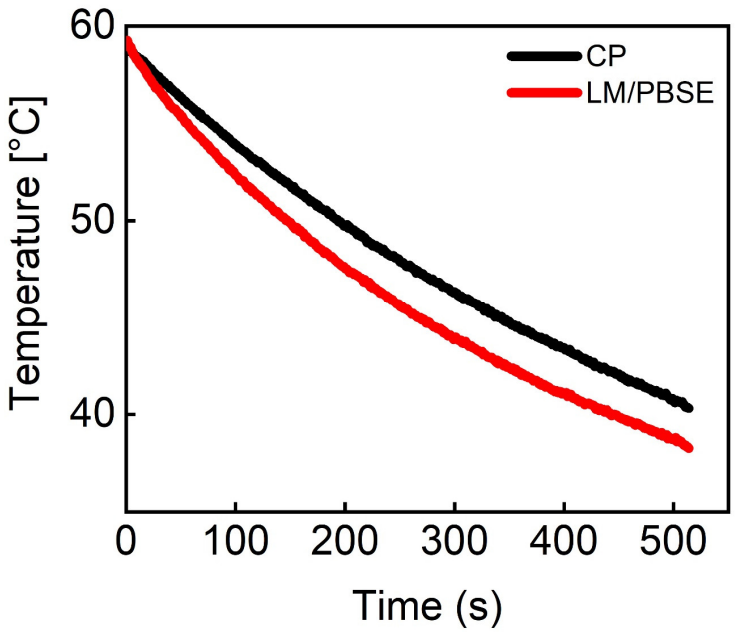

Figure S18. The heat dispersion ability of CP and LM/PBSE.

Movie S1.
The comparison of the crack morphology for pure PBSE matrix and LM/PBSE elastomer.
Movie S2.
The full-field temperature distributions of the LM/PBSE on the surface of specimens during the heating and cooling process.
Movie S3.
The thermal camouflage ability of the LM/PBSE butterfly.
Movie S4.
The thermal dissipation behavior for XHP LED at the rated voltage between the stretched LM/PBSE matrix and CG matrix.
Movie S5.
The thermal dissipation behavior for XHP LED over the rated voltage between the LM/PBSE matrix and CG matrix.
Movie S6
The LM/PBSE wearable wristband application for outdoor sports at night.
Movie S7
The LM/PBSE wearable wristband application for unpredictable power failure occasions.
Movie S8
The heat dissipation property of the LM/PBSE elastomer and a commercial product.